

RESEARCH ARTICLE

Understanding cure and interphase effects in functionalized graphene-epoxy nanocomposites

Kyriaki Gkaliou¹  | George Trakakis²  | Anastasios Manikas² | Philip R. Davies³ | Jeremy Hall⁴ | Costas Galiotis^{2,5} | Mark J. Eaton⁴

¹Department of Chemical and Biochemical Engineering, The Danish Polymer Center, Kongens Lyngby, Denmark

²Foundation of Research and Technology Hellas, Institute of Chemical Engineering Sciences (ICE-HT), Patras, Greece

³Cardiff Catalysis Institute, Cardiff School of Chemistry, Cardiff University, Cardiff, UK

⁴Cardiff School of Engineering, Cardiff University, Cardiff, UK

⁵Chemical Engineering Department, University of Patras, Patras, Greece

Correspondence

Kyriaki Gkaliou, Department of Chemical and Biochemical Engineering, The Danish Polymer Center, Lyngby, 2800, Denmark.
Email: kyrgk@kt.dtu.dk

Funding information

Engineering and Physical Sciences Research Council (EPSRC); EPSRC Industrial Innovation

Abstract

Agglomerations effects of graphene-based nanofillers are often reported in the literature to be the main reason on the deterioration of the mechanical properties, especially at high filler loadings. In our study, we focused on the correlated effects of plasma-treated graphene nanofillers on the curing reaction and mechanical properties of an epoxy matrix. Specifically, we explored the effect of dispersion state, planar size, filler content, surface functionalization and stoichiometric ratio on the epoxy curing process. The surface of the treated graphene nanofillers were studied in detail by X-ray photoelectron spectroscopy (XPS), Raman spectroscopy and X-ray diffraction (XRD). The results indicated greater presence of oxygen containing groups with the crystallinity to be unaffected after the plasma process. Dynamic Mechanical Analysis (DMA) was used to assess the changes in both the T_g and the mechanical properties of graphene-epoxy nanocomposites. Rheological and microscopic data showed that a well-dispersed material was achieved at high filler loadings with the use of calendaring and plasma functionalization. Although, a well-dispersed material was achieved on the bulk composite, no further mechanical reinforcement was observed at high filler loadings. The adsorption of epoxy groups onto the graphene nanofillers' surface, leading to a stoichiometric imbalance between the epoxy chains and hardener molecules, was proposed to explain the results.

KEYWORDS

curing effects, dispersion state, dynamic mechanical analysis, epoxy resin, plasma-treated graphene sheets

1 | INTRODUCTION

Epoxy resin is a well-established thermoset polymer with a wide variety of applications ranging from electronics to aerospace, due to its excellent properties, including stiffness, durability, light weight, low toxicity and low cost.¹ Curing of the epoxies is achieved by the reaction between linear prepolymers and cross-linking agents (hardeners), resulting in a highly crosslinked, three-dimensional macromolecular

structure.² Since the relationship between the structure and properties of the epoxy systems is the foundation of the material design, cured resins with a variety of properties can be obtained by changing the chemical structure of epoxy resins and curing agents,^{3,4} the cure schedule⁵ and the epoxy/hardener ratio in the reaction mixture.^{6,7} One of the properties that can be affected by these factors is the glass transition temperature (T_g), which is the temperature range where a thermosetting polymer changes from a hard, rigid or "glassy" state to

This is an open access article under the terms of the [Creative Commons Attribution](https://creativecommons.org/licenses/by/4.0/) License, which permits use, distribution and reproduction in any medium, provided the original work is properly cited.

© 2023 The Authors. *Polymers for Advanced Technologies* published by John Wiley & Sons Ltd.

a more pliable, compliant or “rubbery” state.⁸ For this reason, understanding the curing process in the epoxy matrix is necessary to optimize the physical properties of the final product.

The addition of nanofillers, like graphene or functionalized graphene nanofillers, to epoxy systems can deliver significant enhancements in properties such as stiffness and strength at very low filler loadings. However, the incorporation of these nanofillers at high filler loadings with the epoxy matrix allows the fillers to interact with the reactive resin and hardener. This results in modified stoichiometry and, consequently, reduced T_g values.^{9–11} According to these reports, the reduction of T_g is mainly due to the following effects; Firstly, the excessive filler loadings of graphene nanofillers act as a barrier, hindering the epoxy/hardener interactions. Secondly, the increase of polymer viscosity which results to the steric effects of the polymer chains and thirdly, the homopolymerisation that occurs between the hydroxylic groups on the graphene surface and the epoxy groups.^{11–13}

On the other hand, a different approach has been suggested by Liu et al.¹⁴ who reported a sharp decline in T_g when increasing the filler loading of nanoalumina in an epoxy system. Specifically, they described the *adsorption effect*, in which epoxy molecules are physically adsorbed on the surface of nanoalumina fillers and create an epoxy-rich interphase that does not react readily with surrounding hardener molecules. Due to the high surface area of these materials, this necessarily creates an amine-rich bulk matrix elsewhere, hence an altered stoichiometry and reduced T_g . A similar *adsorption effect* has been reported for surface-treated carbon fiber-based epoxy composites,^{15–17} highlighting that carbon fiber and graphite surfaces can adsorb curing amine, resulting in a non-stoichiometric composition at the interphase. Therefore, such effects are important to be well understood because any changes to curing could lead to a detrimental effect on composite mechanical properties.

In addition to the curing effects, the mechanical properties of filled polymers and nanocomposites are strongly linked to the adequate dispersion of the nanofiller in the pre-polymer during the composite preparation.^{18–21} It has been reported^{22–26} that above a certain filler loading, the Young's modulus of the final nanocomposites remains stable. Although, these optimum filler loadings can be very low (≤ 1 wt.%), where non-significant flake-to-flake interactions would occur, this effect is often associated with agglomerations resulting in lower stress transfer efficiency. However, these reports have not considered the curing effects, and consequently the relationship between the curing effects and the mechanical reinforcement has not sufficiently investigated, especially regarding to the nanofiller loading.

Clearly the addition of nanofillers to cross-linked epoxy resins has an influence on the curing of the base polymer. If the matrix properties are diminished compared to an unfilled material, then the expected composite properties will not be achieved, and the reinforcing effect of the nanofillers could be somewhat masked. Therefore, this study sets out to establish a better understanding of the effect graphene based nanofillers have on the curing of the epoxy systems and to evaluate their impact on the mechanical properties of the matrix. The influence of key parameters, such as filler loading, dispersion state, planar size and stoichiometry have been explored.

2 | EXPERIMENTAL

2.1 | Materials

Three graphene powders were investigated in this study. Two, “few layer graphene” (FLG) powders were supplied by Haydale Ltd; an unfunctionalized FLG “pristine” and the same FLG material, plasma treated in a COOH atmosphere (HDPlas[®]GNPs). The third material was rGO (partially reduced GO) supplied by Avanzare. Detailed chemical and morphological characterizations are included on the Supplementary Section S1. According to the suppliers' data sheets, the planar size and the thickness of FLG materials is ~ 8 and 2 nm, respectively. The rGO has a planar size of ~ 40 μm and thickness of < 3 nm. Table 1 represents the thickness of the materials via XRD and TEM data (as described at Supplementary Information S1) in comparison with the suppliers' information.

A commercial resin system supplied by Easy Composites Ltd, (“IN2 epoxy infusion resin”, 1,6-bis (2,3-epoxypropoxy)hexane, epichlorohydrin-formaldehyde-phenol polymer and bisphenol-A(epichlorohydrin) modified epoxy resin). The infusion resin was catalyzed using the Easy Composites Ltd. AT30 fast hardener (cycloaliphatic and aliphatic amine-based mixture) with a ratio of 100:30, giving a pot-life of 9–14 min, a gelation time of 2–4 h and is de-mouldable in around 6 h.

2.2 | Preparation of graphene-epoxy nanocomposites

Nanocomposites of FLG, FLG-COOH and rGO from 0.25 to 2 wt.% were manufactured using two different mixing methods. Maximum

Samples	d -Spacing (nm)	β , FWHM (°)	Thickness (nm)		Suppliers' data (nm)
			XRD	TEM	
FLG	0.3548	3.07 ± 0.102	2.71	4.26 ± 1.30	2
FLG-COOH	0.3694	3.47 ± 0.07	2.35	2.8 ± 0.9	2
rGO	-	-	-	1.73 ± 0.49	< 3

TABLE 1 Thickness from XRD and TEM analysis of FLG, FLG-COOH and rGO.

Note: The measured thickness from the XRD data was calculated using the Scherrer equation.²⁷

concentrations of 2 wt. % and 0.5 wt.% for rGO were reached due to the high viscosity of the systems containing FLG, FLG-COOH and rGO, respectively.

2.2.1 | One step method: Speed mixing method (SM)

Graphene filler was well mixed in IN2 epoxy infusion resin, using a speed mixer (Dual Asymmetric Centrifuge 800.1 FVZ) with a speed of 1950 rpm for 5 min. Then, the mixtures were degassed for around 1 h in a vacuum chamber in order to remove any trapped air.

2.2.2 | Two-step method: Speed mixing method (SM) and three roll mill (TRM)

The same SM procedure as the one step method was followed without degassing. In order to enhance dispersion, a calendaring process was adopted as follows: The dispersion of the filler was performed using an Exakt 80E three roll mill (Exakt GmbH) in two steps. In this system, the narrow gaps can be controlled from 5 to 200 μm between the rollers, combined with the mismatch in angular velocity of the adjacent rollers, result in locally high shear forces with a short residence time. One of the unique advantages of this technique is that the gap width between the rollers can be mechanically or hydraulically adjusted and maintained, thus it is easy to get a controllable and narrow size distribution of particles in viscous materials.

A total of five passes were performed at varying speeds and nip gaps, to gradually breakdown the agglomerates. The three rollers are identified as the feed roller, N_1 , the central roller, N_2 , and the apron roller, N_3 . The ratio of roller speeds for $N_1:N_2:N_3$ is 1:3:9 and the

speed is specified as the rpm of the apron roller (N_3). During the first pass, the apron roller speed was 350 rpm and the gap sizes between roller pairs were: $N_1-N_2 = 45 \mu\text{m}$ and $N_2-N_3 = 15 \mu\text{m}$. For the remaining passes (2-5) the apron roller speed was 450 rpm and the roller gaps were reduced to: $N_1-N_2 = 15 \mu\text{m}$ and $N_2-N_3 = 5 \mu\text{m}$. Then, the mixtures were degassed for 1 h in a vacuum chamber.

After mixing the commercial resin dispersions were mixed with the hardener (AT30) at a ratio of 100:30 (resin: hardener) for 2 min in the SM with speed 1950 rpm and they were degassed again for 10 min as the pot life of the hardener is 15–20 min. For DMA measurements, mixtures were then casted into aluminum molds at room temperature for 6 h and then cured in the oven at 60°C for 12 h. A schematic is presented in Figure 1 that includes all the steps for the fabrication of the composites.

2.3 | Dispersion study

The properties of graphene/epoxy nanocomposites depend greatly on the degree of graphene dispersion and exfoliation in the pre-polymer at the resin preparation level. Rheology has been used in order to evaluate analytically the dispersion and the interconnection of graphene nanofillers in epoxy-based dispersions. Steady shear experiments were conducted in Bohlin C-VOR 200 shear rheometer. A parallel aluminium plate geometry (500 μm gap and 40 mm diameter) was used to analyze the dispersions. The flow properties of the graphene-based epoxy liquids without the addition of hardener were studied using the rheometer in rotational mode. Shear viscosity (η) and shear stress (τ) were recorded in the shear rate range 0.15–1000 s^{-1} . The delay time for each step was 5 (s) and the integration time was 5 (s). All the measurements were performed at 25°C and repeated three times and the average was taken along with the

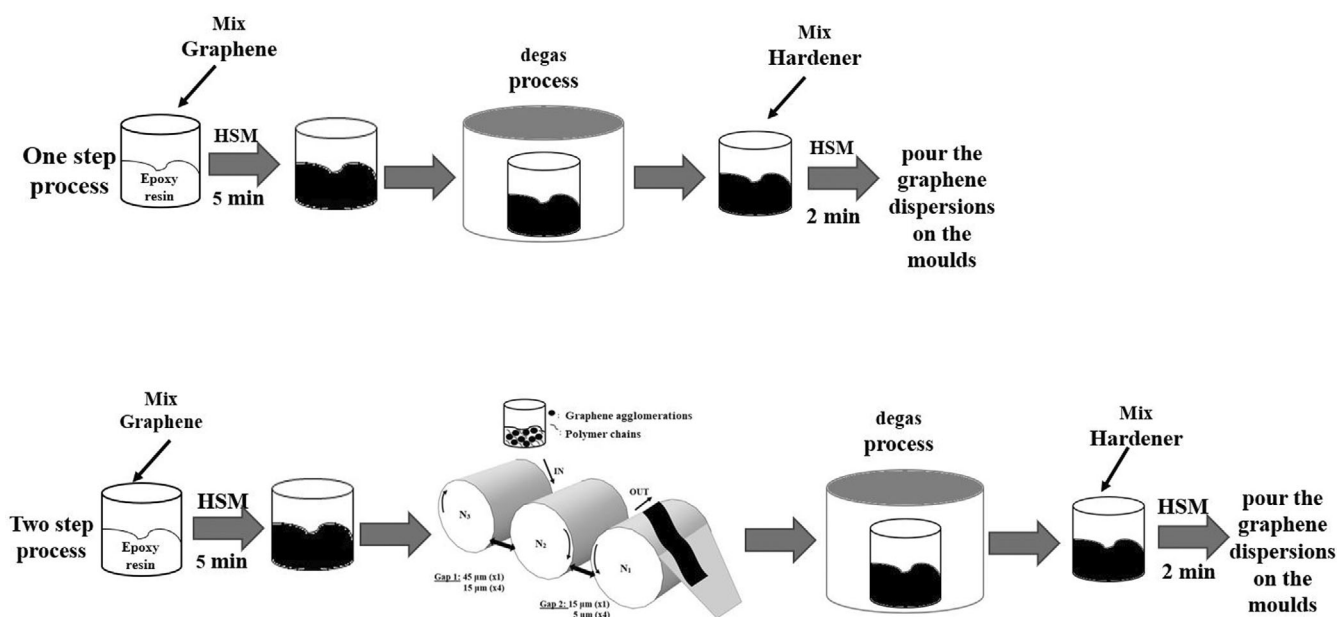


FIGURE 1 Schematic illustration of fabrication methods.

standard deviation. All the rheological parameters were calculated using the Bohlin C-VOR 200 software.

The microstructure analysis of graphene-based epoxy composites was performed by Scanning Electron Microscopy (SEM) analysis. The composites were frozen in liquid nitrogen and then broken manually. The samples have been sputter coated with an overlayer of Au-Pd alloy (BIO-RAD SC500) and their fracture surface was investigated using a Zeiss Sigma HD Field Emission Gun Analytical SEM.

2.4 | Dynamic mechanical analysis (DMA)

DMA was used to provide information about the storage modulus and the tan delta ($\tan \delta$) within the measured temperature range of the functionalized graphene- composites. The temperature at the maximum $\tan \delta$ value was taken as glass-transition temperature (T_g). Dynamic mechanical analysis (DMA) measurements were performed using Perkin Elmer DMA8000, with specimen dimensions of $\sim 17 \text{ mm} \times 5 \text{ mm} \times 2 \text{ mm}$. The single cantilever bending mode with a displacement of 0.05 mm applied at 1 Hz was used for all specimens. The temperature was ramped from room temperature to 140°C at a heating rate of $3^\circ\text{C}/\text{min}$ and a minimum of five specimens were measured for every batch. At room temperature, strain multiplex measurements were also performed using a strain range 0.001–1 mm with a constant frequency 1 Hz. The samples were tested within their linear viscoelastic region (LVR) to ensure low force conditions that do not destroy the polymer structure.²⁸ The choice of the strain (displacement) control for applying

the deforming load to the sample was selected in the range that the dynamic strain and stress showing a linear relationship.²⁹ For all the composites, strain and stress are linearly related and the displacement of 0.05 mm was selected. The analysis was performed using the Perkin Elmer Pyris software. The clamp compliance was investigated and accounted for in the storage modulus calculations in line with the process described by Duncal et al.³⁰ This process is outlined in detail in the Supplementary Information document (Section 2). All the samples were kept in a desiccator between manufacture and testing in order to avoid any moisture absorption.

2.5 | Thermal analysis

A Perkin Elmer TGA/DSC 3+ was used to obtain information on the thermal stability of nanofillers and the nanofiller-based epoxy composites. The samples were measured in aluminum oxide crucibles using a sample weight of $\sim 10\text{--}15 \text{ mg}$ and were heated from 25 to 800°C at the heating rate of $5^\circ\text{C}/\text{min}$ under a nitrogen atmosphere. A minimum of three measurements was repeated for every material.

3 | RESULTS AND DISCUSSION

XPS analysis was conducted in order to study in depth the surface chemical structure and composition of FLG, FLG-COOH and rGO powders used as reinforcements. Figure 2 illustrates the XPS scans in

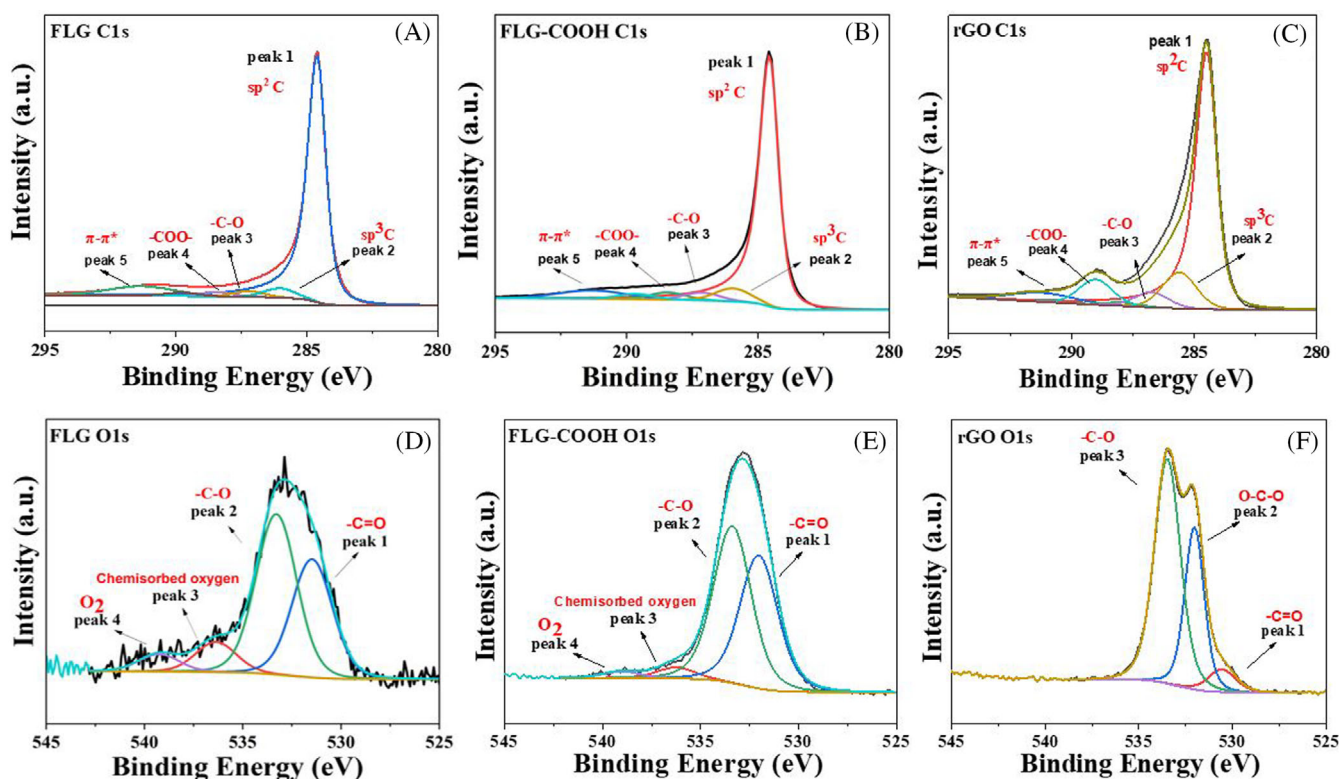


FIGURE 2 XPS C 1s and O 1s scans of FLG (A–D), FLG-COOH (B–E) and rGO (C–F).

the C 1s and O 1s regions. In detail, the C 1s scan (Figure 2A–C) showed the presence of C–C bonding at 284.3 eV (peak 1) binding energy attributed to the graphene structure.³¹ This sample is predominantly graphitic in nature and a fit derived from a pure graphite reference (cluster cleaned HOPG)³² was used as the basis for the graphitic contribution to the C (1s) envelope. The remaining signal can be attributed to carbon–oxygen functionalities, which have been fitted with peaks of similar full width at half maximum (FWHM). Specifically, a peak at 285.6 eV (peak 2) have been attributed to defects in the carbon nanotube structure (sp^3 hybridization) as well as the peaks at 287.4 eV (peak 3) and 289.3 eV (peak 4), corresponding to carbon atoms attached to oxygen groups, $-C=O$ and $-COO$ ($O-C=O$), respectively.^{33,34} Finally, the $\pi-\pi^*$ transition loss peak was detected at 291.3 eV (peak 5), which indicates that the delocalized π conjugation is restored in graphene sheets.³⁵ Regarding the O 1s scan (Figure 2D–F) was fitted to four peaks: peak 1 at 532.1 eV corresponding to the oxygen with a double bond to carbon ($-C=O$), peak 2 at 533.3 eV corresponding to oxygen with a single bond to carbon ($-C-O$),³⁶ peak 3 at 535.9 eV corresponding to the oxygen atoms absorbed on the graphene surface³⁷ and peak 4 at 538 eV originates from oxygen of the residual ambient air. After the plasma process, the O 1s peak of FLG-COOH mainly comes from the residual epoxy groups C–O and carbonyl groups C=O, which is consistent with the analysis on the C 1s spectrum (Figure 2B). In the case of rGO, the O 1s scan (Figure 2F) was fitted mainly with three satellite peaks: peak 1 (530.5 eV) is assigned to double bonded oxygen (C=O), peak 2 (532 eV) is for oxygen atoms with two bonds to carbon (C–O–C) and peak 3 (533.5 eV) is for oxygen atoms with one bond to carbon (C–O).

Finally, XPS survey scan is presented (Figure S1), illustrating the presence of oxygen and carbon elements. The atomic and weight concentrations of each element present on the surface of the graphene nanofillers are summarized in Table 2. Following the XPS analysis, the oxygen contents were found to be 0.98 at.% for untreated FLG, ~6 at.% for FLG-COOH and ~11 at.% for rGO.

Figure 3 represents the FLG, FLG-COOH and rGO/epoxy suspensions in terms of shear viscosity (A, C, E) and stress (B, D, F) as a function of shear rate, respectively. For all samples, a growing shear stress was observed for both increasing shear rates and increasing weight fractions. Shear viscosity has been used as a key-parameter to

optimize the dispersion level; it is a cause effect of the dispersion which becomes high when good dispersion is achieved.³⁸ In our data, up to 0.5 wt.% the viscosity is stable and relatively similar with the pure epoxy resin, which means that these composites are below the percolation threshold with the agglomeration effects to be negligible.

By increasing the concentration to 1 wt.%, there was a general increase on the viscosity for the speed mixed composites in comparison with the other concentrations. Applying the TRM as a mixing method, a transition from Newtonian to shear-thinning behavior was observed, suggesting the existence of a well-dispersed graphene network, which increases the viscosity at rest and low shear rates and breaks up into the isolated particles at higher shear rates. The efficiency of the TRM was also demonstrated in the case of rGO, as shown in Figure 3E,F.

Interestingly, the addition of the plasma-treated material did not raise the viscosity of the system as much as the untreated nanofiller. At a low shear rate region (below $1 s^{-1}$), the values of viscosity of FLG and FLG-COOH were found 6.26 and 2.15 Pa s for the same filler loading (1 wt.%), respectively. As reported by Valley et al.,²³ this different behavior must be related to the existence of different interactions filler–polymer due to the different levels of functionalization. In fact, FLG with a higher C/O atomic ratio than the FLG-COOH provided a higher viscosity and hence a more homogeneous dispersion in the epoxy matrix. These results suggest that the addition of carboxylic groups added after the plasma process does not provide better dispersion on the epoxy system at high filler loadings. On the other hand, the increase of the hydroxylic and epoxy groups ($-C-O$ and $O-C-O$, respectively) on the surface of rGO as well as the higher aspect ratio of rGO (planar size: 40 μm) led to a great enhancement of the viscosity with only 0.5 wt.% rGO mixed by TRM, reaching 31.77 Pa s at low shear rates (below $1 s^{-1}$).

Figures 4 and 5 summarized the morphological investigation performed on a cured state of the nanofillers into the epoxy matrix by using SEM. Comparing the two mixing methods, a more densely packed agglomerates were observed in the case of fracture surface of HSM-mixed composites, as shown in Figure 4A–C and Figure 5A–C. Moreover, a fairly uniform distribution is achieved using the TRM technique for both of materials with the surface roughness to be increased, as presented at Figures 4B–D and 5B–D. This arises due to the better distribution.³⁹ Regarding to the effect of plasma-treatment,

TABLE 2 Atomic and weight percentage of surface element composition for all the samples.

Sample	Element (at.%)					Oxygen content (at.%)					(wt.%)	
	$-C=O$	$-C-O$	$O-C-O$	Chemisorbed oxygen	O_2	Oxygen (O 1s)	Carbon (C 1s)	Silicon (Si 2p)	Sulfur (S 2p)	C	O	
FLG	0.36	0.48	-	0.09	0.36	0.98	99.02	-	-	98.69	1.30	
FLG-COOH	2.42	2.87	-	0.20	0.12	5.61	94.39	-	-	92.65	7.34	
rGO	0.73	6.88	3.72	-	-	11.33	88.07	0.24	0.09	85.35	14.64	

Note: The calculation was performed from the O 1s and C 1s high resolution XPS spectra.

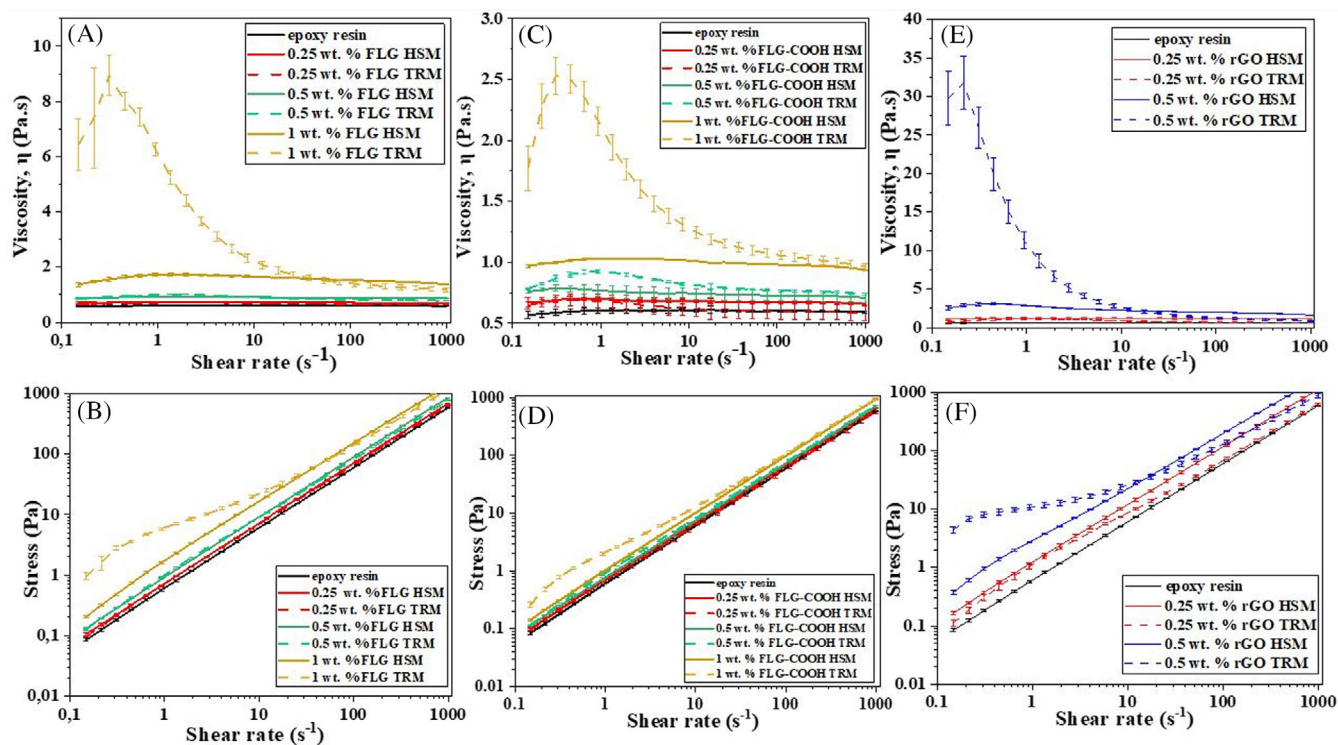


FIGURE 3 Steady shear curves (shear viscosity and stress as a function of shear rate) of FLG (A, B), FLG-COOH (C, D) and rGO (E, F) dispersions in epoxy resin at different concentrations.

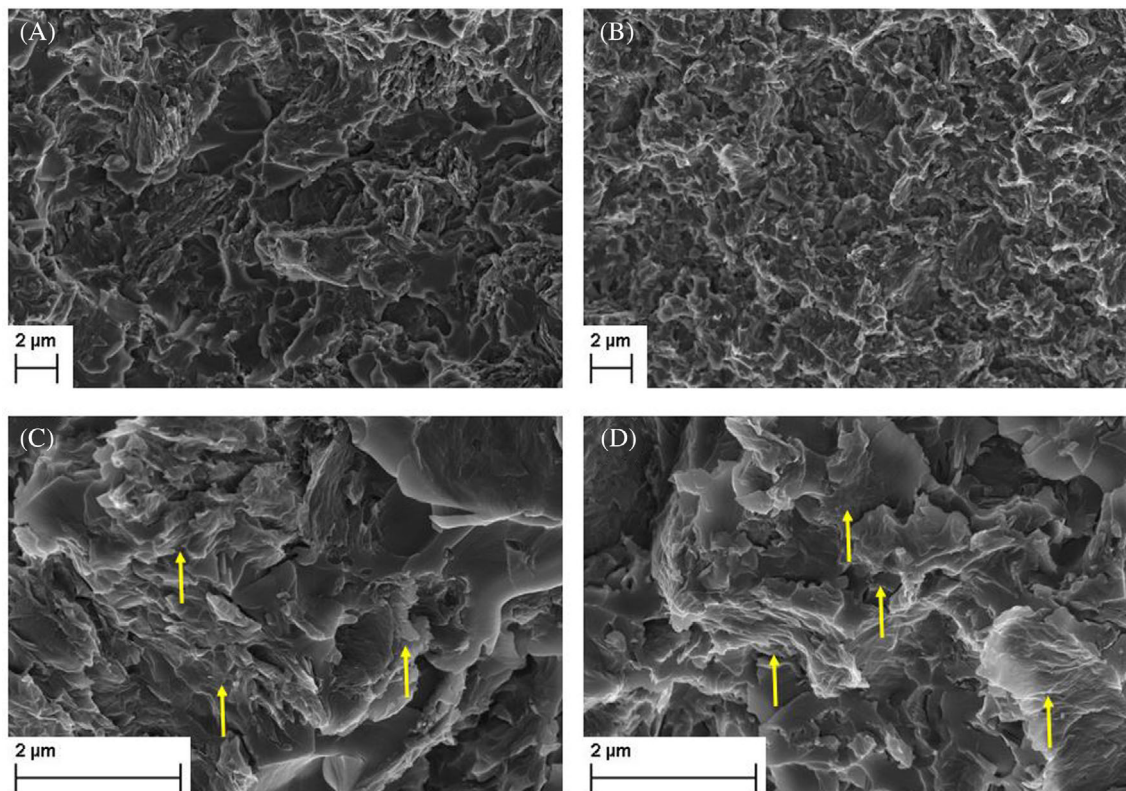


FIGURE 4 SEM images of fracture surface of 2 wt.% FLG/epoxy composites mixed by HSM (A, C) and TRM (B, D). Yellow arrows have been used in order to highlight the wrinkle surface of few layer graphene sheets.

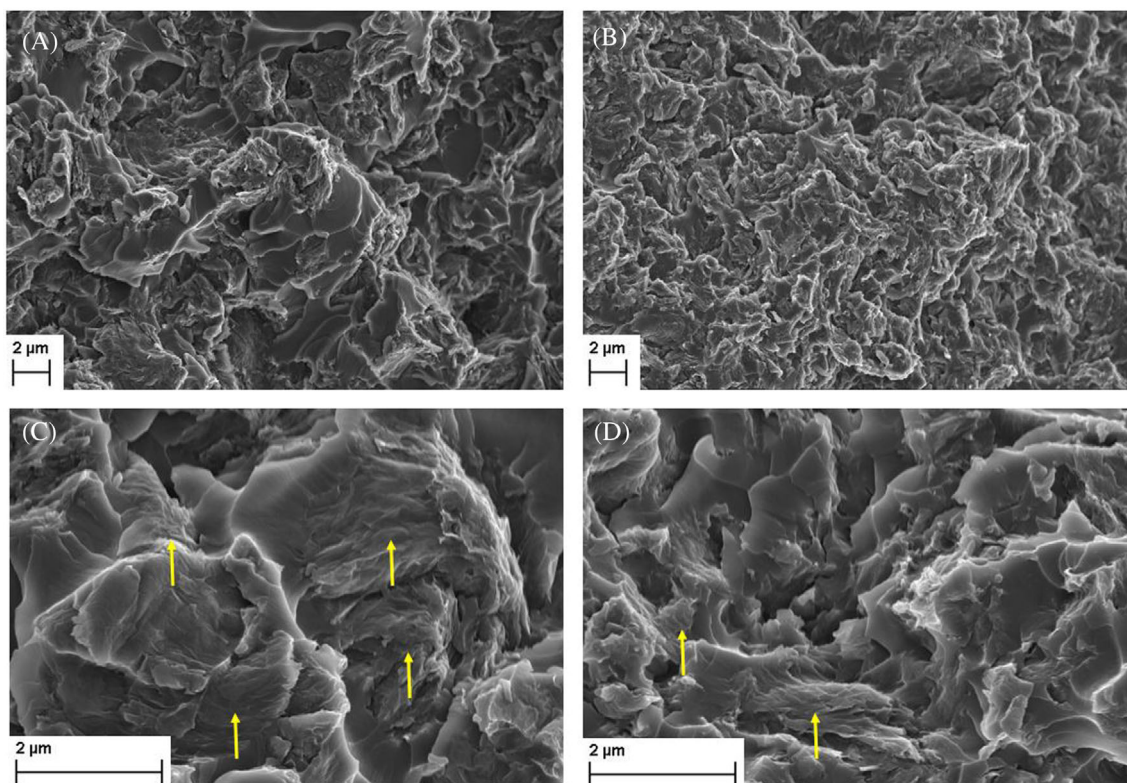


FIGURE 5 SEM images of fracture surface of 2 wt.% FLG-COOH/epoxy composites mixed by HSM (A, C) and TRM (B, D). Yellow arrows have been used in order to highlight the wrinkle surface of few layer graphene sheets.

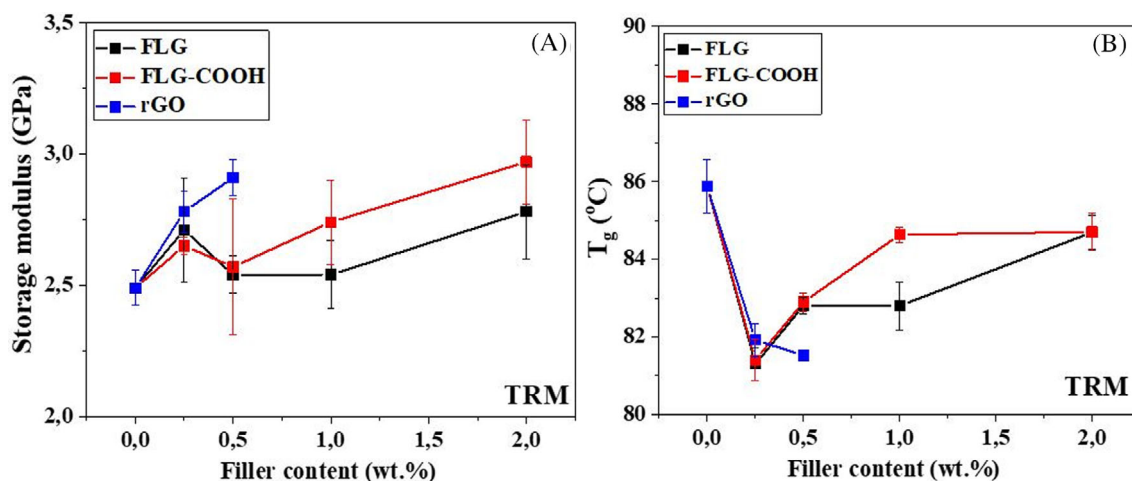


FIGURE 6 Storage modulus at 30°C (A), T_g (B) values for FLG, FLG-COOH and rGO/epoxy nanocomposites, respectively as a function of nanofiller concentration prepared by TRM mixing method.

it was difficult to identify the differences between the dispersion of FLG and FLG-COOH. However, some agglomerations were observed (Figure 5D), indicating the difficulty to overcome the high adhesive van der Waals forces despite the high shear forces applied by TRM.

Figure 6 illustrates the variation of storage modulus (A), T_g (B) and loss modulus (C) for pure epoxy and its composites reinforced with FLG, FLG-COOH and rGO, as a function of the filler concentration. Similar results are obtained for the composites mixed by SM, as

presented in Supplementary Information Figure S6. By introducing 0.25 wt.% of FLG, FLG-COOH and rGO, an initial increase in storage modulus in the range of 5%–10% is observed but no significant improvement (plateau effect) in storage modulus was observed after increasing the nanofiller concentration any further. A similar effect of filler concentration was reported by Valles et al.,²³ in which the mechanical properties of the GO/epoxy nanocomposites deteriorated after the optimum loading of 1 wt.%. Similarly, Li et al.⁴⁰ reported a

best interfacial stress transfer in 0.2 wt.% GO/epoxy nanocomposite, with a decrease observed upon increasing the filler loading to 0.5 and 1 wt.%. Both of reports suggest that this deterioration was attributed to agglomerations occurring at higher filler loadings. However, in our results, good dispersion has been demonstrated across the high filler loadings and functionalized fillers, as proved by rheology and SEM. For this reason, this study focused on the curing effects to the mechanical properties rather than the agglomerations effects.

In contrast to the results presented in the literature,¹⁰ which show the T_g decreasing at higher filler loadings (due to the steric hindrance of the molecular activity), here, the addition of only 0.25 wt.% of the nanofillers leads to a significant drop of T_g ($\sim 5^\circ\text{C}$). In fact, at 0.5 wt.% of rGO, the T_g decreases further while in case of FLG and FLG-COOH, the T_g slightly increases, indicating that higher amount of oxygen groups in the surface of rGO affects the curing of the epoxy system. This shows that in this case, the nanomaterials have affected the curing reaction of the epoxy system even at low concentrations and this likely correlates to specific surface area, that is, the same mass fraction of a high surface area material will increase steric hindrance compared with a lower surface area material. Hence

comparing filler loadings by weight might not be that helpful when considering curing effects.

The effect of the incorporation of nanofillers on the curing reaction was also confirmed by TGA analysis, where a drop in initial decomposition temperature (IDT) was seen for all three materials after the addition of only 0.25 wt.% filler, as shown in Figure 7 (Table S2 includes in detail the thermal properties of the composites). As the T_g has been reduced with the filler incorporation, the cross-linking network of the epoxy system is affected, resulting in thermal degradation at lower temperatures. The IDT of all composites gradually begins to recover as the filler concentration is increased, but it does not exceed that of the pure epoxy. An improved dispersion is achieved between the nanofiller and the polymer matrix at high fillers, as a result the mobility of the local matrix around the nanofillers is reduced, offering a better barrier effect. This prevents the degradation of the epoxy matrix and results in higher degradation temperatures,⁴¹ as shown in Figure 7C.

In our case, these curing effects can explain why only very modest improvements in storage modulus are seen as the filler loading increases. In other words, the T_g drops at lower filler loadings,

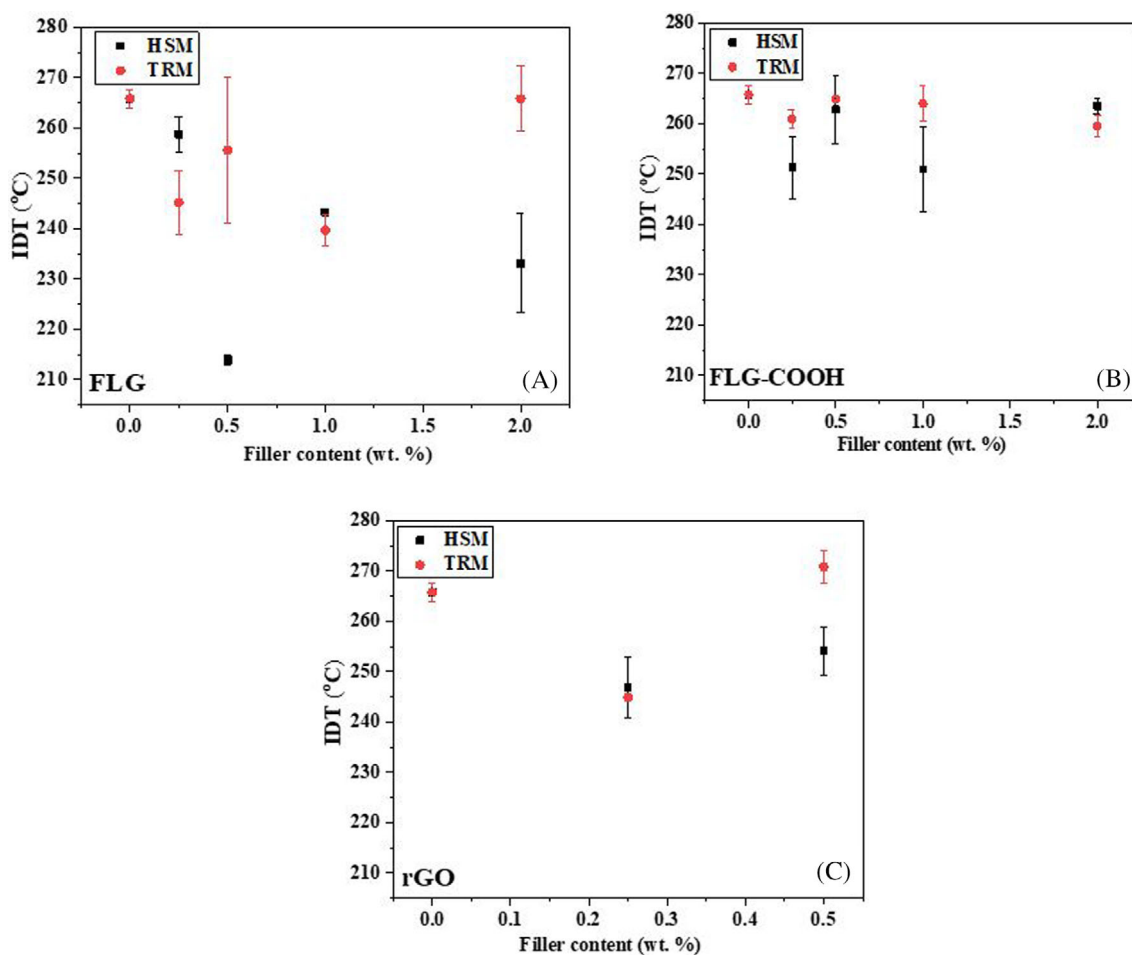


FIGURE 7 Initial decomposition temperature (IDT) values of FLG (A), FLG-COOH (B) and rGO (C)/nanocomposites as a function of filler content, mixed by HSM and TRM methods.

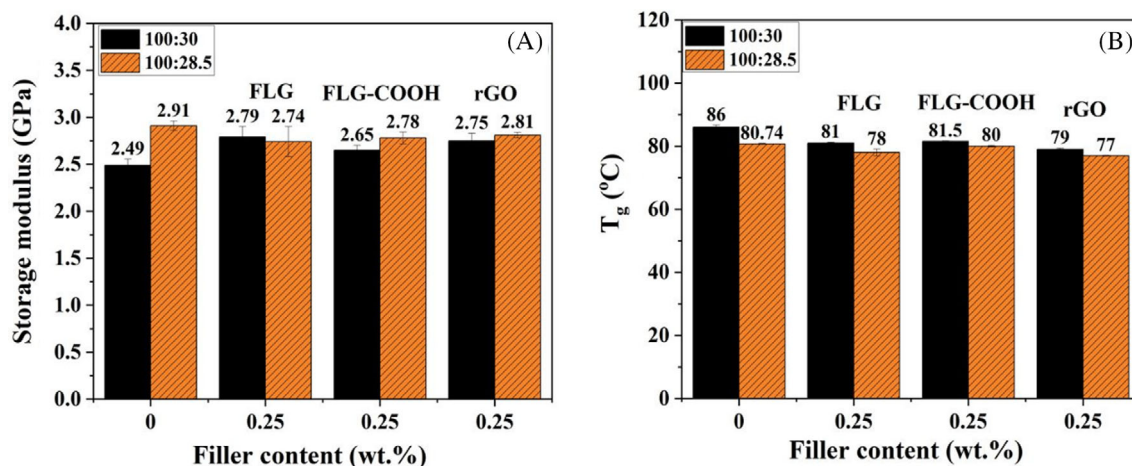


FIGURE 8 Storage modulus at 30°C (A) and T_g (B) values for 0.25 wt.% FLG, 0.25 wt.% FLG-COOH and 0.25 wt.% rGO by ratio 100:30 (black bars) and 100:28.5 (orange bars).

suggesting more molecular motion and hence lower modulus, but as filler loading increases T_g recovers as the graphene restricts molecular motion and finally enhances the modulus, but not significantly. Specifically, the oxygen content on the surface of FLG, FLG-COOH and rGO, which was detected by XPS can explain the curing effects seen. The surface functionalization of the graphene can catalyze the ring opening curing.^{10,11} This leads to a lower cross-linking density around the filler interphase and hence an epoxy-rich environment in the interphase region, due to the reduced mobility of the epoxy molecules around the nanofillers. In addition of this, Vanlandigham et al.⁴² showed that for an unfilled epoxy system with a non-stoichiometric ratio, a two-phase microstructure forms consisting of a “hard” phase (formed by initial reactions), surrounded by a “soft” phase (consisting of unreacted and partially reacted species), with the properties highly dependent on the soft phase. If we assume that in our systems, a two-phase structure has formed at the filler interphase due to the *adsorption effect* of epoxy groups on the graphene surface, this mechanism supports the DMA data observed.

If the assumption above is correct, reducing the hardener ratio will lead to a higher change in T_g for the nanocomposites due to epoxy-rich environment in the interphase region and by having lower amount of hardener molecules, the lack on the amine groups is higher. This will allow us to understand better the surface effect of the nanofillers to the stoichiometric ratio. Therefore, we reduced the hardener component by 5%. Figure 8A,B shows the storage modulus and T_g values of 0.25 wt.% FLG, FLG-COOH and rGO with two different hardener ratios (100:30 and 100:28.5). Only the HSM method was used in this experiment as similar trends were seen for both TRM and HSM.

When the unfilled epoxy was cured using the non-stoichiometric ratio, the T_g dropped by 5°C which is comparable with the reduction in T_g that results from the addition of fillers at the correct stoichiometric ratio (100:30), as shown in Figure 8B. This supports the suggestion that the stoichiometric composition is disrupted by the presence of the nanofillers, with the hardener molecules not able interact with the polymer chains, resulting in a reduced cross-linking

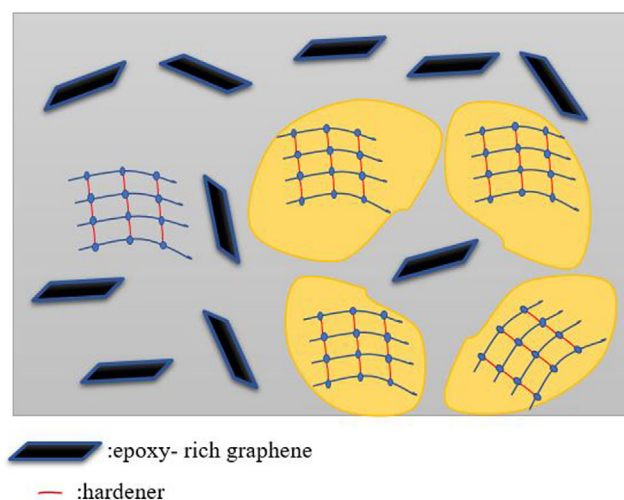


FIGURE 9 A schematic representation showing the microstructure of the epoxy nanocomposites. The yellow parts represent the soft phase on the bulk composite created by the unreacted hardener molecules.

density. Additionally, the T_g of filled composites reduces further when the non-stoichiometric ratio is used (100:28.5) because the nanofillers are continuously affected the curing through the *adsorption effect*.

According to the results presented at Figure 8A, a moderate positive effect was found on the storage modulus of the non-stoichiometric composites in comparison with the stoichiometric composites. By decreasing the amine content below the stoichiometric ratio, the polymer network tends to have a reduced dense structure with more linear chains, which enhances the efficiency of load transfer among the polymer chains⁴² and consequently, the modulus of the polymer increases.

A possible schematic of the microstructure in the bulk composites is represented at Figure 9. In the case of the stoichiometric graphene-composite (100:30), the graphene nanofillers are physically absorbed the epoxy chains (epoxy-rich graphene), leading to the reduction of T_g and hence, a non-stoichiometric network is surrounded by a soft

phase (the unreacted hardener molecules, amine-rich environment). Therefore, a lower reinforcement was observed on the bulk composite. When the amount of hardener is reduced (100:28.5), the epoxy-rich interphase remains similar while the amine-rich environment (soft phase) decreases, leading to an increase on the modulus.

4 | CONCLUSIONS

The main conclusion of this study is that the structural and geometrical characteristics of graphene nanomaterials leads to a major modification of both the microstructure and mechanical properties of the polymer when they are incorporated. In the literature, the deviation of the theoretical and the experimental modulus values are often attributed to the effects of agglomerations, but this study suggests curing effects can have a significant impact on the mechanical properties at high filler loadings as confirmed by DMA analysis. By adjusting the stoichiometric ratio and achieving a well-dispersed material, a reduced cross-linking density was confirmed in the case of FLG, FLG-COOH and rGO/epoxy nanocomposites. It is suggested that the physically adsorption effect of epoxy chains onto the graphene surface leads to a non-stoichiometric balance and thus diminished mechanical properties at high loading. These results provide valuable insights for understanding the effect of graphene nanomaterials on the interphase region within the epoxy matrix and its influence on the mechanical properties of the bulk nanocomposites.

ACKNOWLEDGMENTS

The authors would like to thank Engineering and Physical Sciences Research Council (EPSRC) for funded my PhD research. Also, we are grateful to EPSRC Industrial Innovation for funded my 3-month placement at Foundation of Research and Technology (FORTH), Hellas.

DATA AVAILABILITY STATEMENT

The data that support the findings of this study are available from the corresponding author upon reasonable request.

ORCID

Kyriaki Gkaliou  <https://orcid.org/0000-0001-5893-4402>

George Trakakis  <https://orcid.org/0000-0003-2779-9900>

REFERENCES

1. Surnova A, Balkaev D, Musin D, Amirov R, Dimiev AM. Fully exfoliated graphene oxide accelerates epoxy resin curing, and results in dramatic improvement of the polymer mechanical properties. *Compos B Eng*. 2019;162:685-691.
2. Pascault J-P, Sautereau H, Verdu J, Williams RJJ. *Thermosetting Polymers*. CRC Press; 2002.
3. Cheng X, Chen Y, Du Z, Zhu P, Wu D. Effect of the structure of curing agents modified by epoxidized oleic esters on the toughness of cured epoxy resins. *J Appl Polym Sci*. 2011;119:3504-3510.
4. Su W, Chen KC, Tseng SY. Effects of chemical structure changes on thermal, mechanical, and crystalline properties of rigid rod epoxy resins. *J Appl Polym Sci*. 2000;78:446-451.
5. Sahagun CM, Morgan SE. Thermal control of nanostructure and molecular network development in epoxy-amine thermosets. *ACS Appl Mater Interfaces*. 2012;4:564-572.
6. Bignotti F, Pandini S, Baldi F, de Santis R. Effect of the resin/hardener ratio on curing, structure and glass transition temperature of nano-filled epoxies. *Polym Compos*. 2011;32:1034-1048.
7. Alhabill FN, Ayoob R, Andritsch T, Vaughan AS. Influence of filler/matrix interactions on resin/hardener stoichiometry, molecular dynamics, and particle dispersion of silicon nitride/epoxy nanocomposites. *J Mater Sci*. 2018;53:4144-4158.
8. Michel M, Ferrier E. Effect of curing temperature conditions on glass transition temperature values of epoxy polymer used for wet lay-up applications. *Construct Build Mater*. 2020;231:117206.
9. Bao C, Guo Y, Song L, Kan Y, Qian X, Hu Y. In situ preparation of functionalized graphene oxide/epoxy nanocomposites with effective reinforcements. *J Mater Chem*. 2011;21:13290-13298.
10. Tian J, Yang C, Yang J, Hao S. The correlated effects of filler loading on the curing reaction and mechanical properties of graphene oxide reinforced epoxy nanocomposites. *J Mater Sci*. 2021;56:3723-3737.
11. Vryonis O, Virtanen STH, Andritsch T, Vaughan AS, Lewin PL. Understanding the cross-linking reactions in highly oxidized graphene/epoxy nanocomposite systems. *J Mater Sci*. 2019;54:3035-3051.
12. Monteserín C, Blanco M, Aranzabe E, et al. Effects of graphene oxide and chemically-reduced graphene oxide on the dynamic mechanical properties of epoxy amine composites. *Polymers (Basel)*. 2017;9:449.
13. Galpaya DGD, Fernando JFS, Rintoul L, et al. The effect of graphene oxide and its oxidized debris on the cure chemistry and interphase structure of epoxy nanocomposites. *Polymer (Guildf)*. 2015;71:122-134.
14. Liu G, Zhang H, Zhang D, Zhang Z, An X, Yi X. On depression of glass transition temperature of epoxy nanocomposites. *J Mater Sci*. 2012;47:6891-6895.
15. Palmese GR, McCullough RL. Effect of epoxy-amine stoichiometry on cured resin material properties. *J Appl Polym Sci*. 1992;46:1863-1873.
16. Pérez-Pacheco E, Moreno-Chulim MV, Valadez-González A, Rios-Soberanis CR, Herrera-Franco PJ. Effect of the interphase microstructure on the behavior of carbon fiber/epoxy resin model composite in a thermal environment. *J Mater Sci*. 2011;46:4026-4033.
17. Garton A, Stevenson WTK, Wang SP. The crosslinking of epoxy resins at interfaces. V. Amine-cured resins at carbon and graphite surfaces. *J Polym Sci A Polym Chem*. 1988;26:1377-1391.
18. Shen M-Y, Chang T-Y, Hsieh T-H, et al. Mechanical properties and tensile fatigue of graphene nanoplatelets reinforced polymer nanocomposites. *J Nanomater*. 2013;2013:565401.
19. Prolongo SG, Moriche R, Jiménez-Suárez A, Sánchez M, Ureña A. Advantages and disadvantages of the addition of graphene nanoplatelets to epoxy resins. *Eur Polym J*. 2014;61:206-214.
20. Cha J, Kim J, Ryu S, Hong SH. Comparison to mechanical properties of epoxy nanocomposites reinforced by functionalized carbon nanotubes and graphene nanoplatelets. *Compos B Eng*. 2019;162:283-288.
21. Pu S, Hao Y-B, Dai X-X, Zhang P-P, Zeng J-B, Wang M. Morphological, rheological, crystalline and mechanical properties of ethylene-vinyl acetate copolymer/linear low-density polyethylene/amphiphilic graphene oxide nanocomposites. *Polym Test*. 2017;63:289-297.
22. Hashim UR, Jumahat A, Jawaid M. Mechanical properties of hybrid graphene Nanoplatelet-Nanosilica filled unidirectional basalt fibre composites. *Nanomaterials*. 2021;11:1468.
23. Vallés C, Beckert F, Burk L, Mülhaupt R, Young RJ, Kinloch IA. Effect of the C/O ratio in graphene oxide materials on the reinforcement of epoxy-based nanocomposites. *J Polym Sci B*. 2016;54:281-291.
24. Li Z, Young RJ, Wang R, et al. The role of functional groups on graphene oxide in epoxy nanocomposites. *Polymer (Guildf)*. 2013;54:5821-5829.

25. Liu T, Zhao Z, Tjiu WW, Lv J, Wei C. Preparation and characterization of epoxy nanocomposites containing surface-modified graphene oxide. *J Appl Polym Sci*. 2014;131(9).
26. Chatterjee S, Nafezarefi F, Tai NH, Schlagenhaut L, Nüesch FA, Chu BTT. Size and synergy effects of nanofiller hybrids including graphene nanoplatelets and carbon nanotubes in mechanical properties of epoxy composites. *Carbon N Y*. 2012;50:5380-5386.
27. Scherrer P. Bestimmung der inneren Struktur und der Größe von Kolloidteilchen mittels Röntgenstrahlen. *Chemische Technologie in Einzeldarstellungen*. 1912;387-409.
28. Dunson D. EAG Appl Note. 2017.
29. Menard KP, Menard NR. *Dynamic Mechanical Analysis*. CRC Press; 2020.
30. Duncan J. Principles and applications of mechanical thermal analysis. *Princ Appl Therm Anal*. 2008;2:119-163.
31. Kang N, Khondaker SI. The impact of carbon sp² fraction of reduced graphene oxide on the performance of reduced graphene oxide contacted organic transistors. *Appl Phys Lett*. 2014;105:1771.
32. Morgan DJ. Cluster cleaned HOPG by XPS. *Surf Sci Spectra*. 2017;24:24003.
33. Zhang H-B, Wang J-W, Yan Q, Zheng W-G, Chen C, Yu Z-Z. Vacuum-assisted synthesis of graphene from thermal exfoliation and reduction of graphite oxide. *J Mater Chem*. 2011;21:5392-5397.
34. Zhou J, Song H, Ma L, Chen X. Magnetite/graphene nanosheet composites: interfacial interaction and its impact on the durable high-rate performance in lithium-ion batteries. *RSC Adv*. 2011;1:782-791.
35. Lin T, Chen J, Bi H, et al. Facile and economical exfoliation of graphite for mass production of high-quality graphene sheets. *J Mater Chem A Mater*. 2013;1:500-504.
36. Pantea D, Darmstadt H, Kaliaguine S, Sümmchen L, Roy C. Electrical conductivity of thermal carbon blacks. *Carbon N Y*. 2001;39:1147-1158.
37. Plomp AJ, Su DS, de Jong KP, Bitter JH. On the nature of oxygen-containing surface groups on carbon nanofibers and their role for platinum deposition—An XPS and titration study. *J Phys Chem C*. 2009;113:9865-9869.
38. Tadmor Z, Gogos CG. *Principles of Polymer Processing*. John Wiley & Sons; 2006.
39. Chandrasekaran S, Sato N, Tölle F, Mülhaupt R, Fiedler B, Schulte K. Fracture toughness and failure mechanism of graphene based epoxy composites. *Compos Sci Technol*. 2014;97:90-99.
40. Li Z, Young RJ, Kinloch IA. Interfacial stress transfer in graphene oxide nanocomposites. *ACS Appl Mater Interfaces*. 2013;5:456-463.
41. Wan Y-J, Tang L-C, Gong L-X, et al. Grafting of epoxy chains onto graphene oxide for epoxy composites with improved mechanical and thermal properties. *Carbon N Y*. 2014;69:467-480.
42. Vanlandingham MR, Eduljee RF, Gillespie JW Jr. Relationships between stoichiometry, microstructure, and properties for amine-cured epoxies. *J Appl Polym Sci*. 1999;71:699-712.

SUPPORTING INFORMATION

Additional supporting information can be found online in the Supporting Information section at the end of this article.

How to cite this article: Gkaliou K, Trakakis G, Manikas A, et al. Understanding cure and interphase effects in functionalized graphene-epoxy nanocomposites. *Polym Adv Technol*. 2023;1-11. doi:[10.1002/pat.6114](https://doi.org/10.1002/pat.6114)